Highly Dispersed Sn-beta Zeolites as Active Catalysts for Baeyer-Villiger Oxidation: The Role of Mobile, *In Situ* Sn(II)O Species in Solid-State Stannation

Elise Peeters,[a] *Guillaume Pomalaza,*[a] *Ibrahim Khalil,*[a] *Arnaud Detaille,*[b] *Damien P. Debecker,*[b] *Alexios P. Douvalis,*[c,d] *Michiel Dusselier*,*[a] *and Bert F. Sels*,*[a]

[a] Centre for Sustainable Catalysis and Engineering (CSCE), Leuven Chem&Tech, KU Leuven, Celestijnenlaan 200F, 3001 Heverlee, Belgium

[b] Institute of Condensed Matter and Nanosciences (IMCN), Université catholique de Louvain (UCLouvain), Place Louis Pasteur 1, Box L4.01.09, 1348 Louvain-La-Neuve, Belgium

[c] Mössbauer Spectroscopy & Physics of Materials Laboratory, Department of Physics, University of Ioannina, 45110 Ioannina, Greece

[d] Institute of Materials Science and Computing, University Research Center of Ioannina (URCI), 45110 Ioannina, Greece

*Corresponding authors:

michiel.dusselier@kuleuven.be

bert.sels@kuleuven.be

A. FIGURES

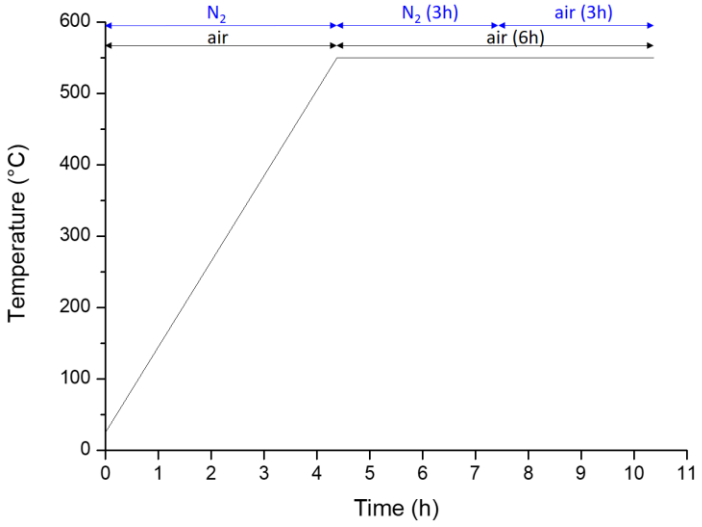

Figure S1. Temperature profile during heat treatment. Double arrows indicate the gas-atmosphere used (black, air; blue, N_2/air).

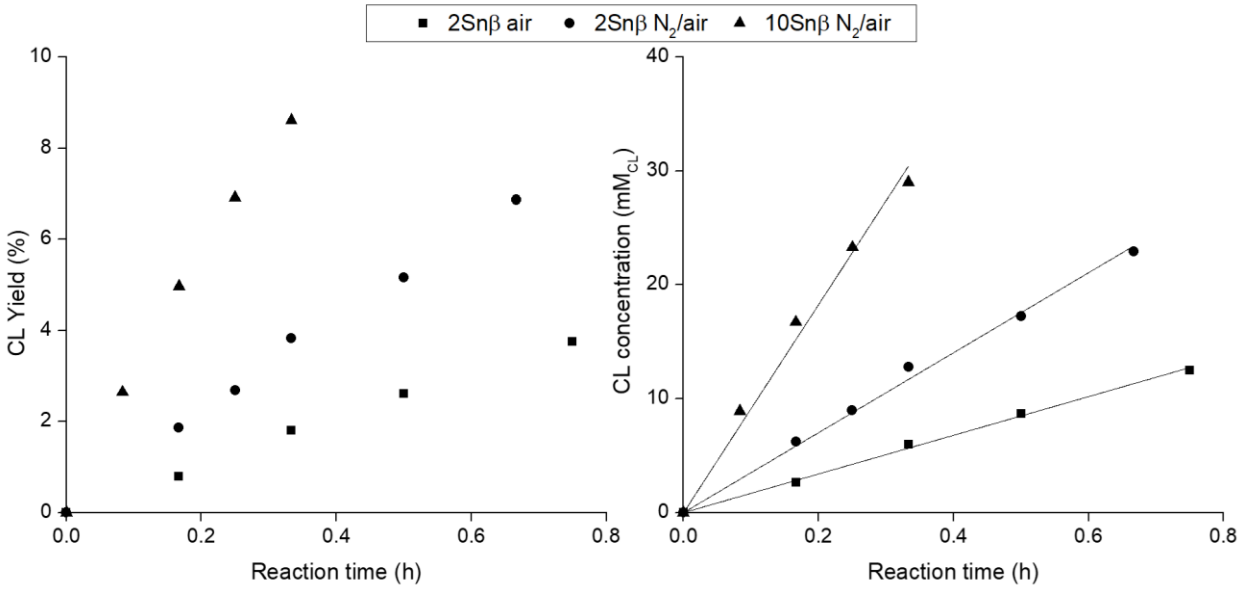

Figure S2. Kinetic plots for various catalysts for the first order BVO reaction of cyclohexanone (CHO) to ε-caprolactone (CL). The yield (left) and concentration (right) of CL are given in function of reaction time. For the initial formation rate, the slope of the linear fit ($R^2 > 0.98$) through the initial points of the CL concentration were calculated. Only the CL concentration data points were used when the CL yield (left) was below 10%. Reaction conditions: cyclohexanone with 50 wt % H_2O_2 at 80°C in dioxane, ratio H_2O_2/ketone = 1.5; c_{ketone} = 330 mM; 10 mg catalyst; 700 rpm.

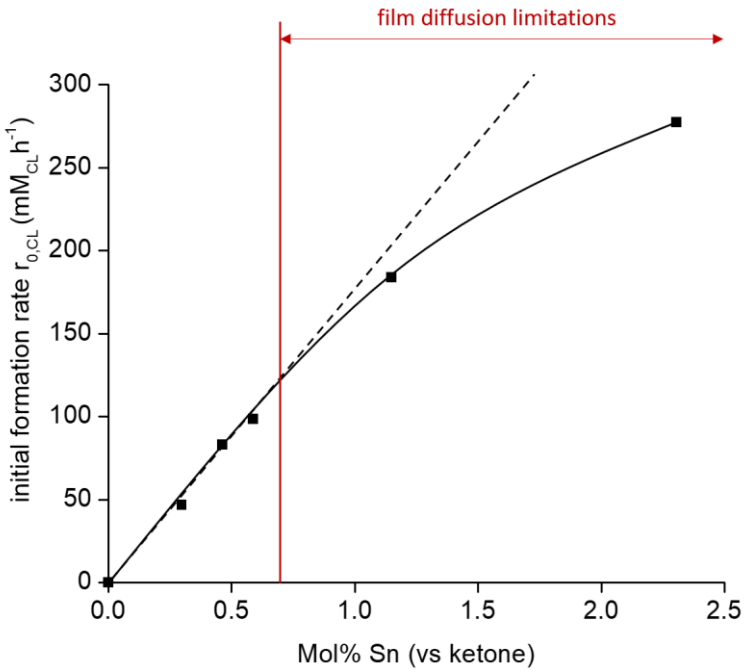

Figure S3. Initial formation rate ($r_{0,CL}$) of CL as a function of Sn concentration (in mol.% Sn relative to the initial ketone substrate) for the BVO of CHO with 10Snβ-N_2/air. To vary the Sn concentration, only the amount of catalyst was changed while all other parameters were kept constant. Reaction conditions: ketone (330 mM in dioxane), H_2O_2 (50 wt % in dioxane), ratio H_2O_2/ketone = 1.5, 80°C and 700 rpm.

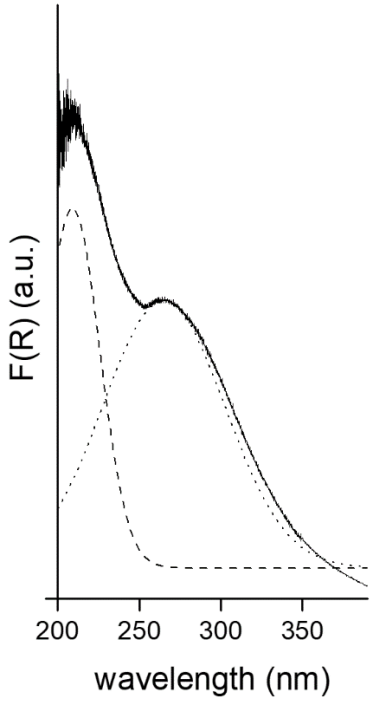

Figure S4. DRUV-Vis spectrum of 10Snβ-air with the fitted deconvolution bands of framework and extra-framework Sn.

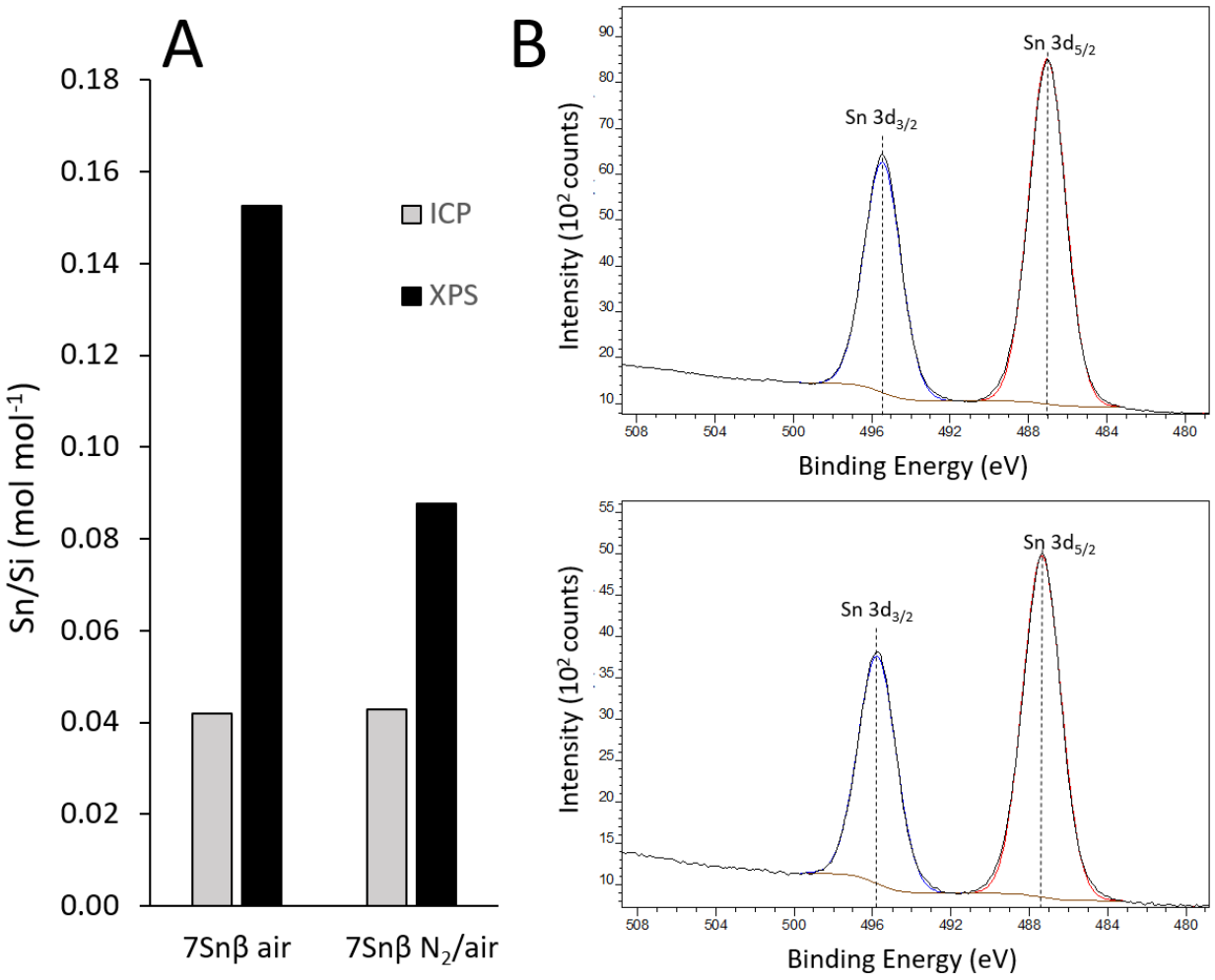

Figure S5. (A) Bulk and surface Sn content (in wt %) as measured by ICP (grey) and XPS (black), respectively, for 7Snβ-(N_2/)air catalysts. **(B)** Illustrative XPS spectrum with indication of the Sn $3d_{3/2}$ and Sn $3d_{5/2}$ peaks for 7Snβ-air (top) and 7Snβ-N_2/air (bottom).

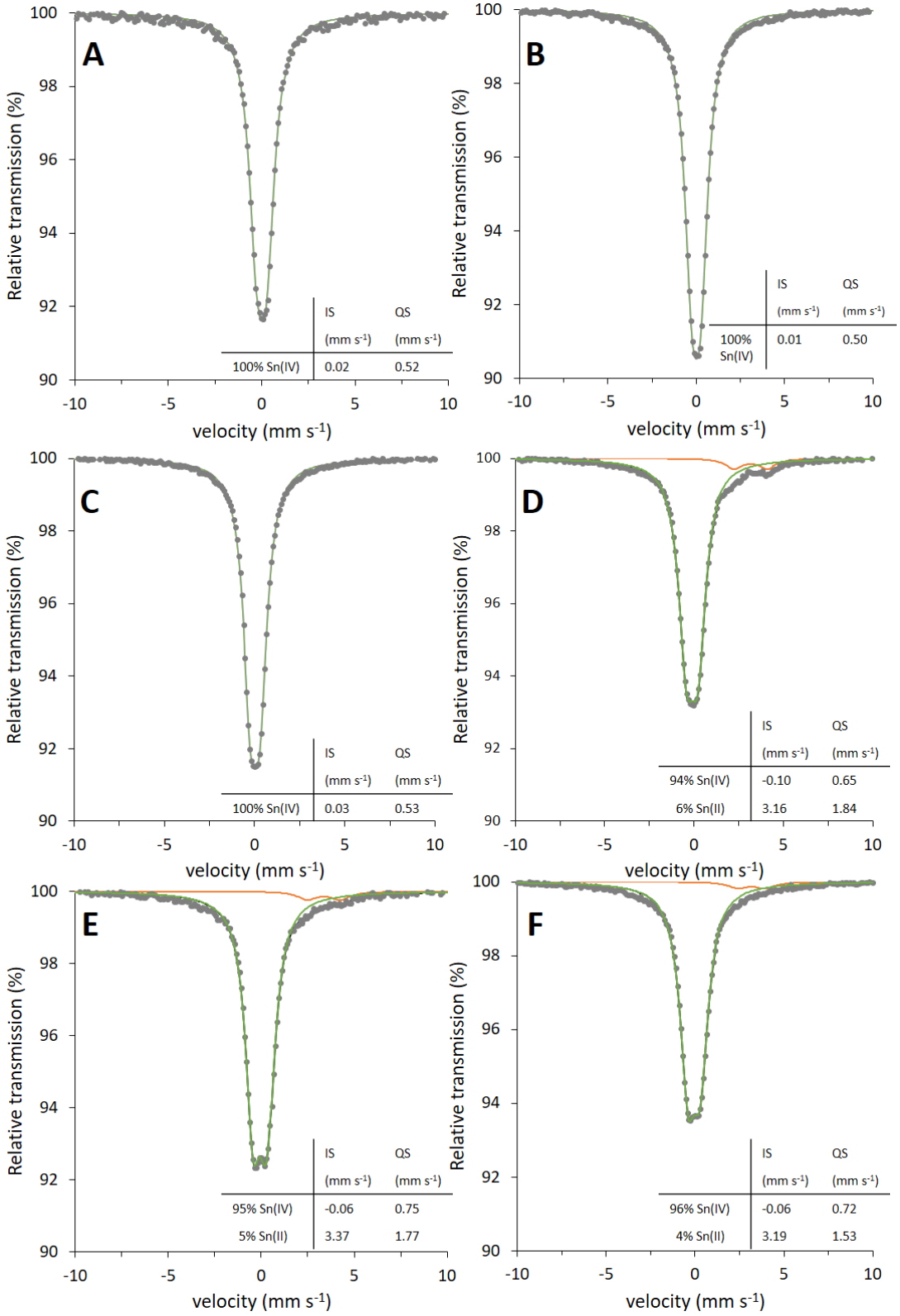

Figure S6. ^{119}Sn Mossbauer spectra recorded at 77 K of **(A)** 2Snβ-air, **(B)** 5Snβ-air, **(C)** 10Snβ-air, **(D)** 2Snβ-N_2/air, **(E)** 10Snβ-N_2/air (3 h air) and **(F)** 10Snβ-N_2/air (6 h air). The points correspond to the experimental data and the colored continuous lines to the components used to fit the spectra (green, Sn(IV); orange, Sn(II)). Percentages of Sn(IV) and Sn(II) are given in the inset table together with the corresponding quadrupole splitting (QS) and isomer shift (IS).

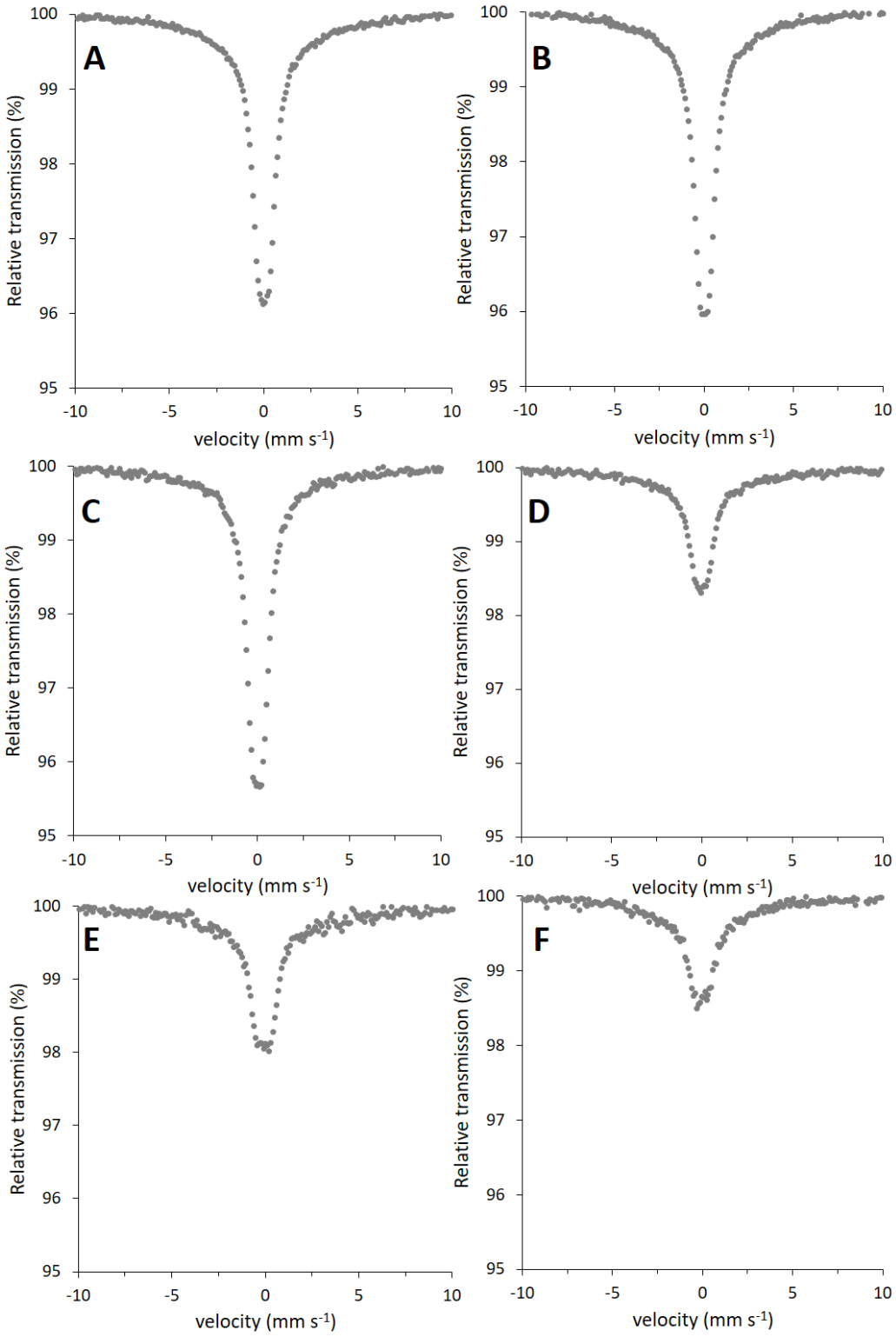

Figure S7. Raw ^{119}Sn Mossbauer spectra recorded at RT of **(A)** 2Snβ-air, **(B)** 5Snβ-air, **(C)** 10Snβ-air, **(D)** 2Snβ-N_2/air, **(E)** 10Snβ-N_2/air (3 h air) and **(F)** 10Snβ-N_2/air (6 h air). The points correspond to the experimental data.

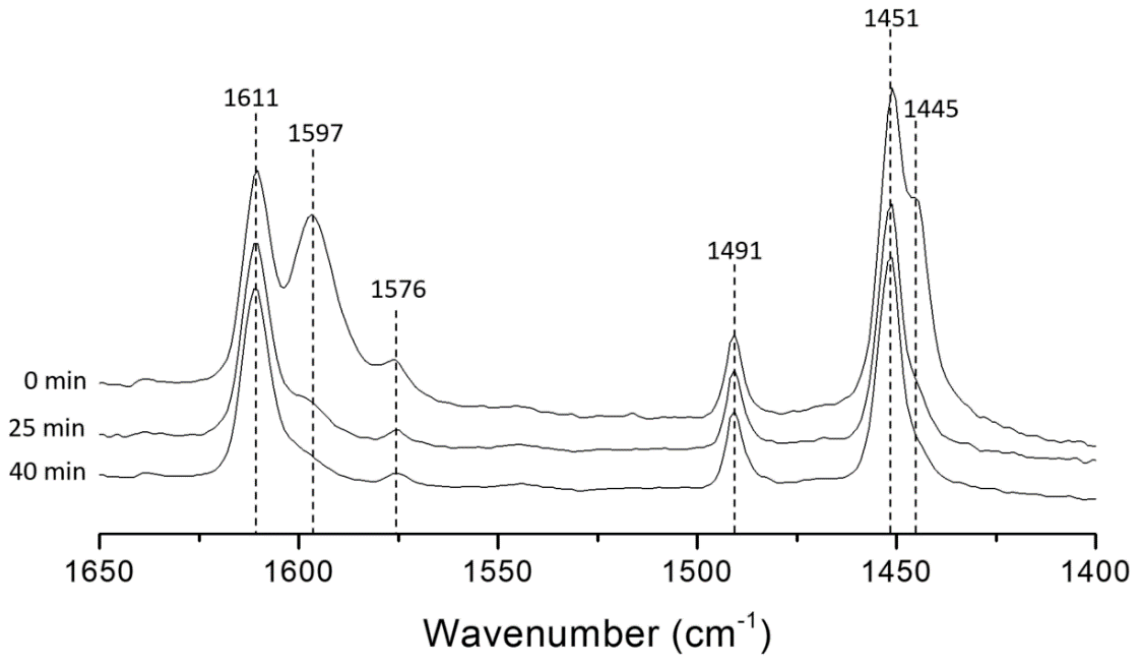

Figure S8. Py-FTIR spectra of 5Snβ-air during exposure to dynamic vacuum at 150°C after 0, 25 and 40 minutes. Dashed reference lines at 1611, 1491 and 1451 cm^{-1} are shown for Lewis acid sites and 1597, 1576 and 1445 cm^{-1} correspond to H-bonded pyridine. To calculate the total amount of Lewis acid Sn-sites, the area of 1451 cm^{-1} of the spectrum measured after 40 min at 150 °C was integrated and used in the Lewis acid density formula (see Materials & Methods). If after 40 min, a band was still present at 1445 cm^{-1} (H-bonded pyridine), deconvolution was performed prior integration.

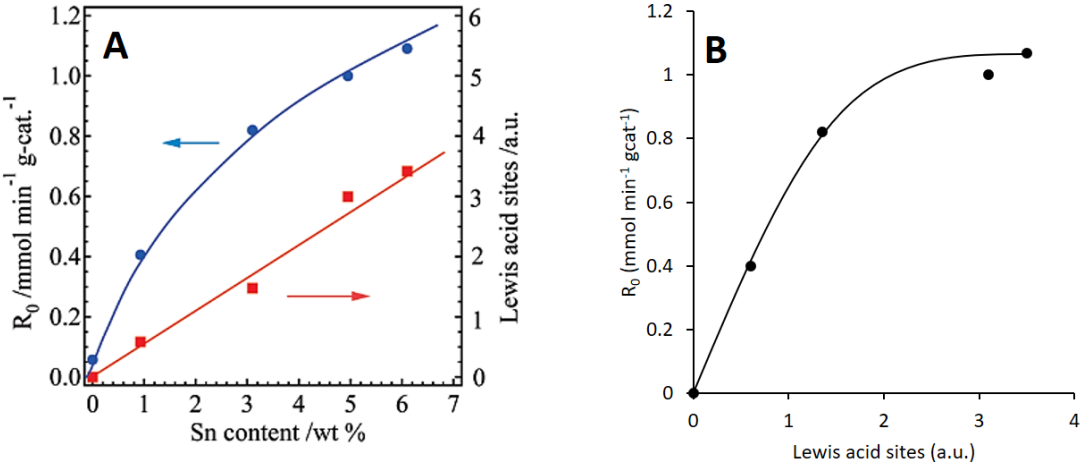

Figure S9. (**A)** Dependence of the initial reaction rate of 2-adamantanone oxidation and the Lewis acid density on the Sn content in Sn-Beta-PS. **(B)** Results of (**A)** converted to R_0 in function of Lewis acid sites to indicate plateau formation. Reproduced with permission from reference 1. Copyright (2011) American Chemical Society.

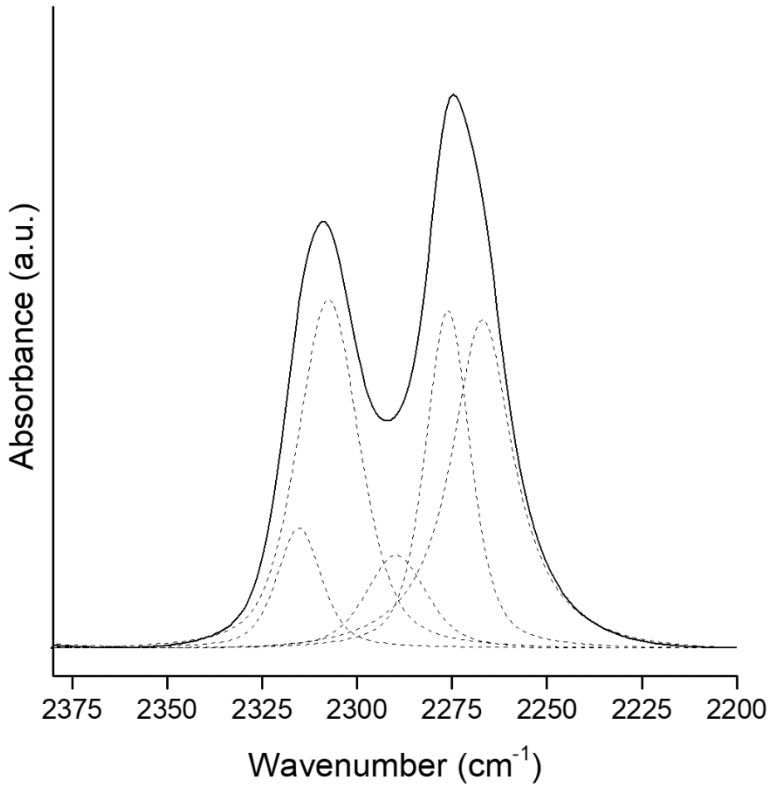

Figure S10. FTIR spectrum of 10Snβ-N_2/air (solid line) after CD_3CN saturation and its deconvolution components (dashed lines) assigned to open Sn sites (2316 cm^{-1}), closed Sn sites (2308 cm^{-1}), SnO_2 (2290 cm^{-1}), SiOH groups (2276 cm^{-1}) and gas-like CD_3CN (2264 cm^{-1}).[2]

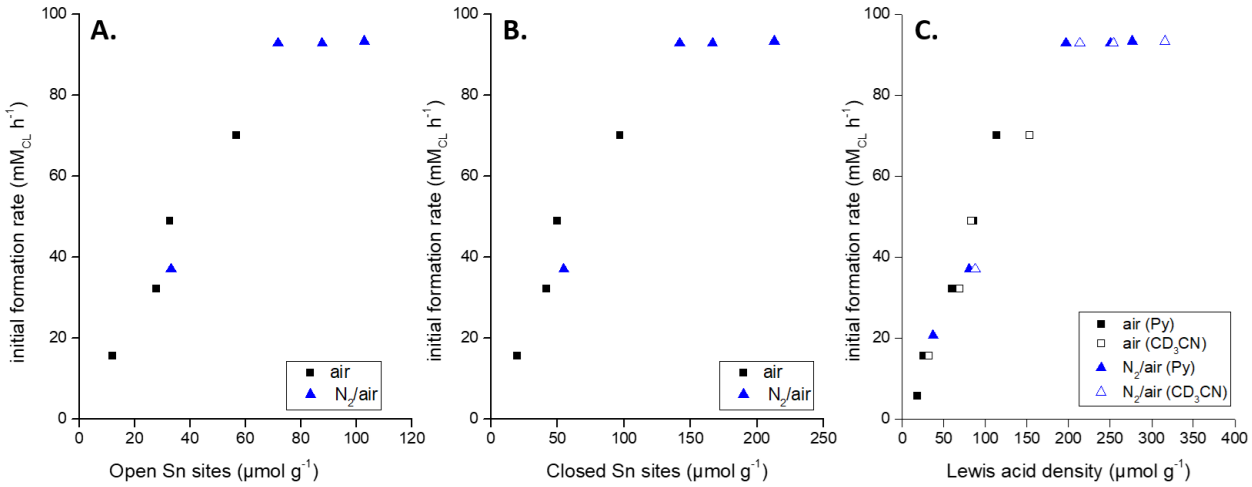

Figure S11. Initial formation rate of CL in relation with **(A)** open Sn sites **(B)** closed Sn sites and **(C)** total amount of Lewis acid sites, determined via Py and CD_3CN-FTIR. The amount of open and closed Sn sites is calculated via CD_3CN-FTIR (see Materials & Methods).[2]

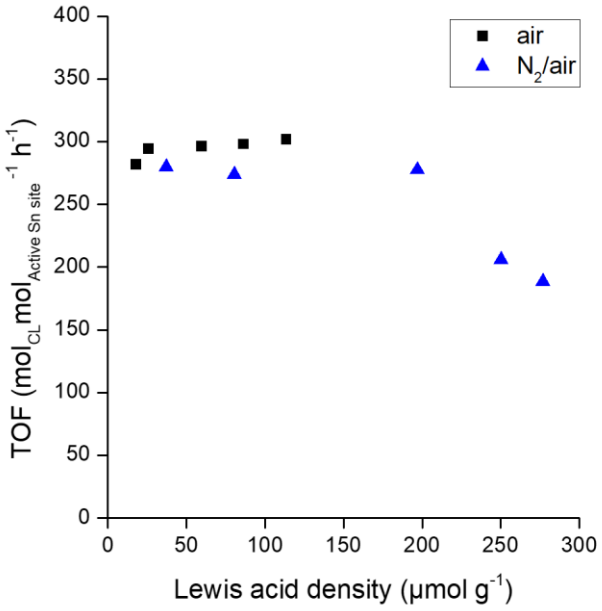

Figure S12. The turnover frequency (TOF) of Snβ catalysts in relation to the Lewis acid density and heating atmosphere applied during SSI (air: black squares, N_2/air: blue triangles). Reaction conditions BVO: Snβ (10 mg), CHO (330 mM in dioxane), H_2O_2 (50 wt % in dioxane), ratio H_2O_2/ketone = 1.5, 80°C and 700 rpm. TOF is calculated by the amount of CL (mol) formed after 10 minutes of reaction, divided by the reaction time and amount of active Sn sites (mol). The total amount of active Sn sites is determined by Py-FTIR by assuming 1 active Sn-site per adsorbed molecule of pyridine.

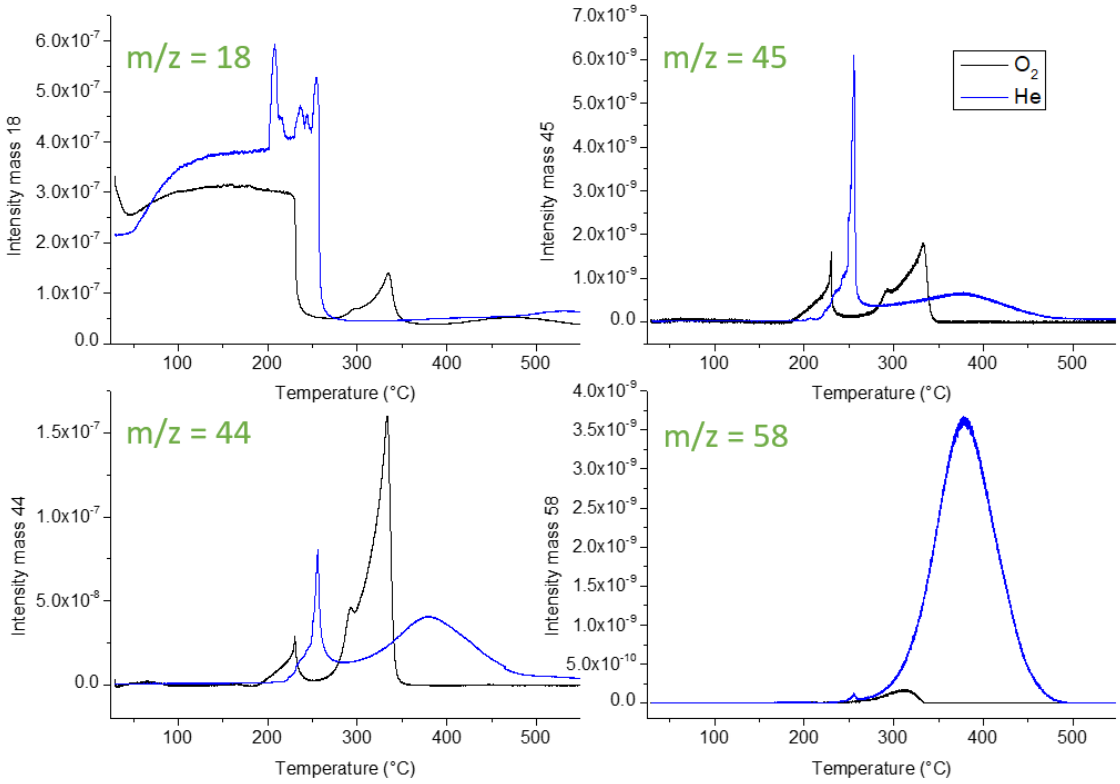

Figure S13. The decomposition products during temperature programmed decomposition (TPDE) with MS of Sn(II) acetate ground with dealuminated β (5 wt % Sn) for both heat treatments. Evolution of water, carbon dioxide, acetic acid and acetone were followed by m/z of 18, 44, 45 and 58, respectively.

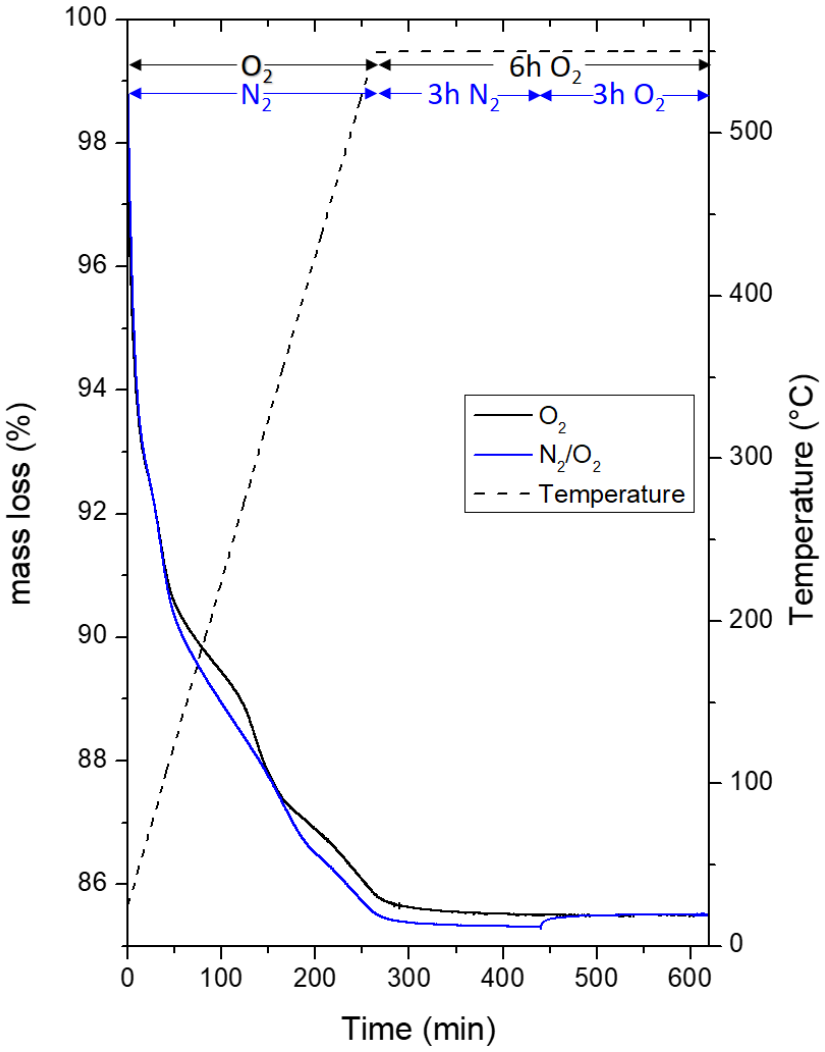

Figure S14. Thermogravimetric analysis of Sn(II)acetate ground with dealuminated β (to obtain final Sn-content of 5 wt %) in O_2 and N_2. All samples were ground for 10 minutes prior to analysis. Full lines refer to mass loss (%) and dashed lines correspond to temperature (°C).

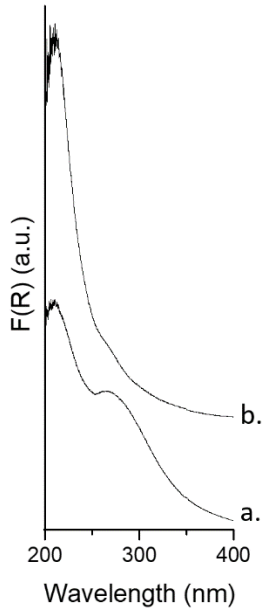

Figure S15. DRUV-Vis of **a.** 5Snβ-190°C_N_2/air (calcined for 3 h at 190 °C in a N_2-flow and 3 h at 550 °C in an air-flow) and **b.** 5Snβ-N_2/air-fast with a heating rate of 10 °C min^{-1} instead of 2 °C min^{-1} to 550°C.

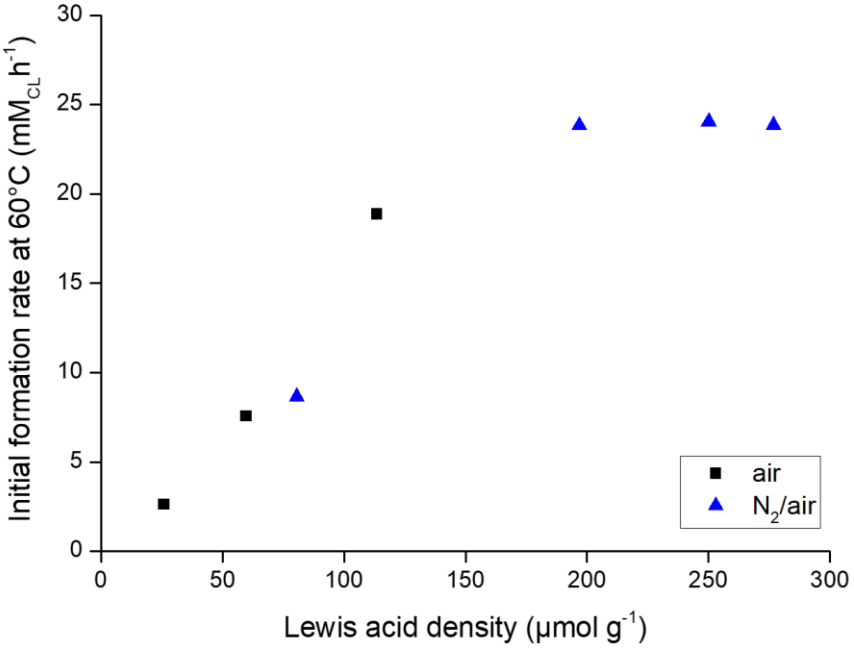

Figure S16. The initial formation rate of CL as function of the Lewis acid density for both heat treatments (air: black squares; N_2/air: blue triangles) at 60°C. The BV oxidation of CHO was performed with 50 wt % H_2O_2 at 60°C in dioxane (ratio H_2O_2/ketone = 1.5 ; c_{ketone} =330mM; 10mg catalyst; 700 rpm). The Lewis acid density was calculated by Py-FTIR at 150°C and 1.42 cm.µmol^{-1} as integrated molar extinction coefficient.[2]

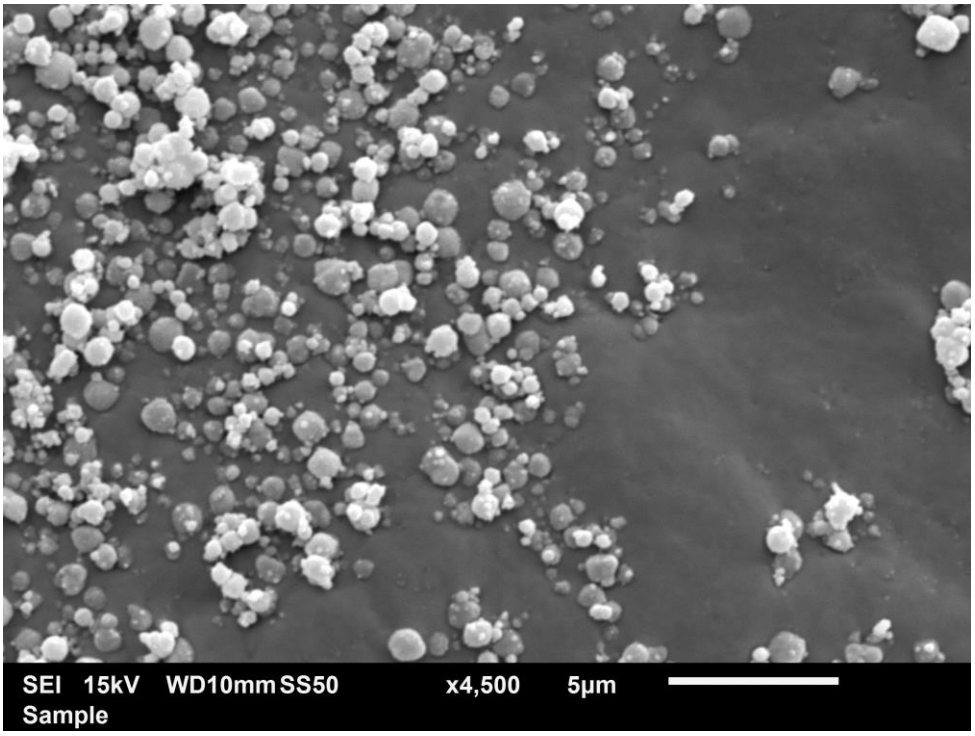

Figure S17. Scanning electron microscope (SEM) image of 10Snβ-N_2/air.

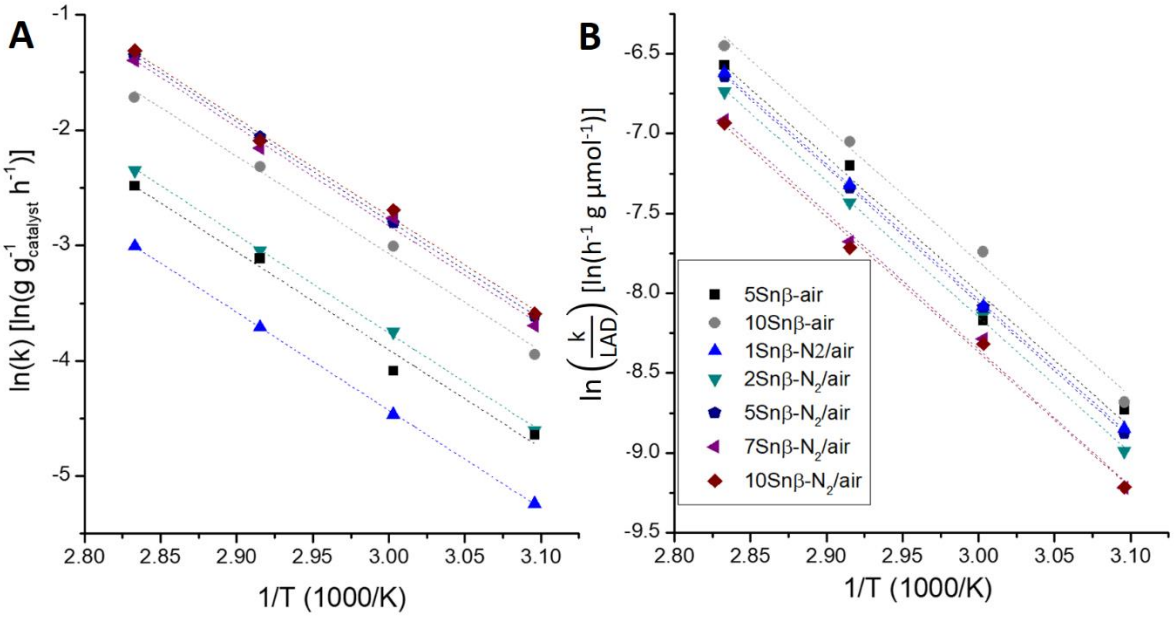

Figure S18. (A) Arrhenius plot for the BVO of cyclohexanone for different Snβ-catalysts. **(B)** modified Arrhenius plot of the k-value divided by the Lewis acid density (LAD, calculated via Py-FTIR).

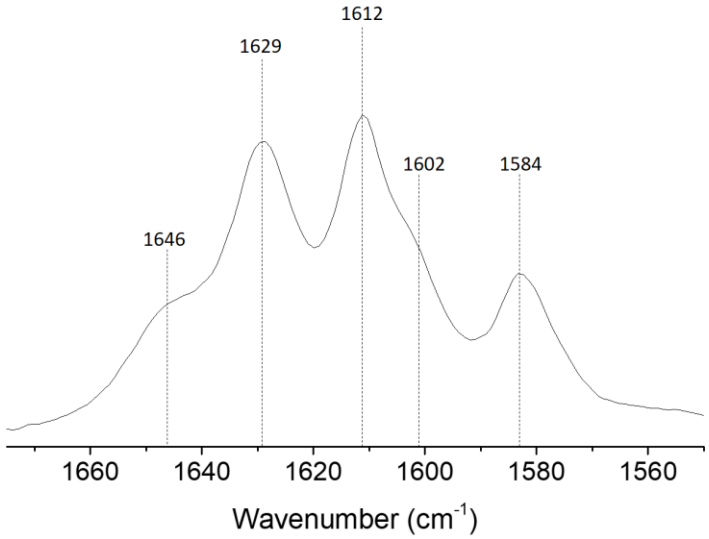

Figure S19. 2,6-Lutidine-FTIR spectrum of 10Snβ-air during exposure to dynamic vacuum at 150 °C after 15 minutes. Dashed reference lines at 1646 and 1629 cm^{-1} refer to H-bonded lutidine and the band at 1612 cm^{-1} corresponds to coordinated lutidine over Lewis acid sites. Hydrogen bonded lutidine or lutidine in interaction with weak Lewis acid sites are characterized by the bands at 1602 and 1584 cm^{-1}.[4,5] To calculate the total amount of Lewis acid Sn-sites, the area of 1612 cm^{-1} of the spectrum measured after 15 min at 150 °C was integrated after deconvolution and used in the Lewis acid density formula (see Materials & Methods).

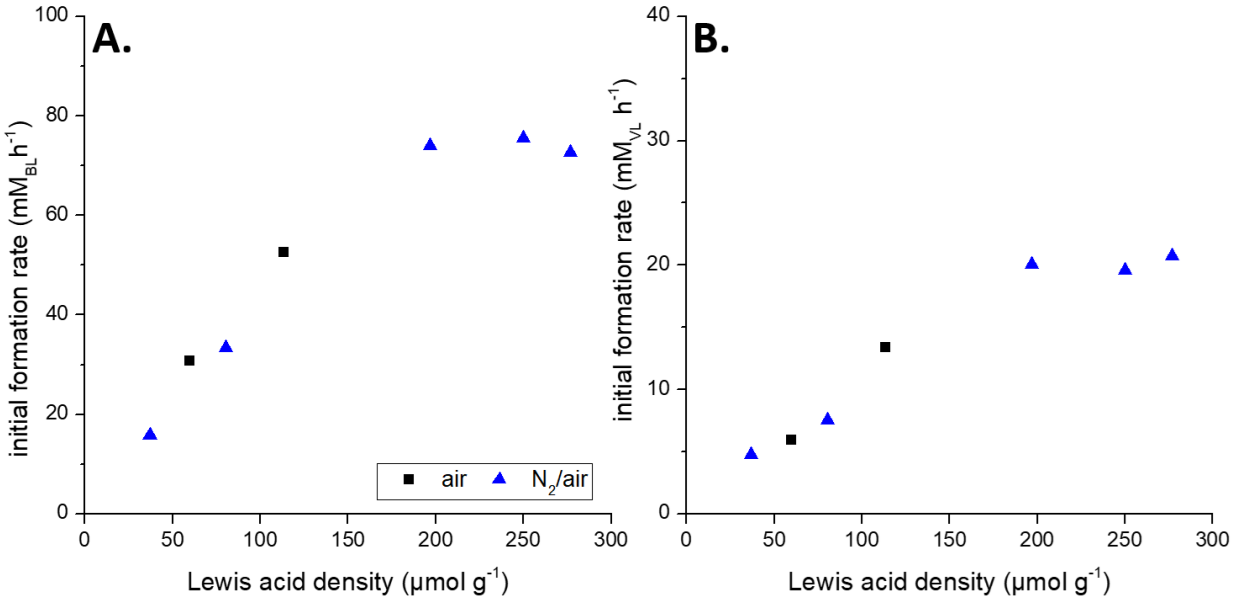

Figure S20. The initial formation rate of butyrolactone (BL) and valerolactone (VL) against LA density starting from **(A)** cyclobutanone and **(B)** cyclopentanone, respectively. Reaction conditions of the BV oxidation of cyclopentanone are identical to the reaction with cyclohexanone at 80°C. For cyclobutanone, the reaction was performed at 20°C with ratio H_2O_2/ketone = 1.5 (50 wt % H_2O_2); c_{ketone} = 330 mM; 10 mg catalyst, in 7.5 mL dioxane.

B. TABLES

Table S1. Physicochemical properties of solid-state Snβ samples

entry	Sample	Sn[a] (wt %)	V_{micro}[b] ($cm^3 \cdot g^{-1}$)	V_{total}[b] ($cm^3 \cdot g^{-1}$)
1.	Hβ-air	-	0.23	0.35
2.	deAlβ-air	-	0.24	0.38
3.	2Snβ-air	1.61	0.21	0.34
4.	5Snβ-air	4.28	0.20	0.34
5.	7Snβ-air	6.27	0.20	0.34
6.	10Snβ-air	9.46	0.19	0.32
7.	2Snβ-N_2/air	1.69	0.21	0.34
8.	5Snβ-N_2/air	4.39	0.20	0.33
9.	7Snβ-N_2/air	6.56	0.19	0.31
10.	10Snβ-N_2/air (3h air)	9.17	0.19	0.32

[a] measured by ICP-AES. [b] calculated via the *t*-plot method.

Table S2. Values for the calculated framework/extra-framework Sn-ratio as measured by DRUV-Vis spectroscopy (left). The normalized area and relative decrease of the silanol region as measured by FTIR spectroscopy of the Snβ samples relative to the calcined dealuminated β-zeolite (right). The spectra were normalized by the total T-O-T overtone area (2100 – 1750 cm^{-1}).[6,7]

	DRUV-Vis	**FTIR**	
Catalyst	Ratio area (210 nm/265 nm)	Normalized area of silanol region (3800 – 3200 cm^{-1})	Relative decrease (%)
Dealβ-air	-	3.91	0
2Snβ-air	0.57	3.35	14.4
5Snβ-air	0.79	2.93	25.1
10Snβ-air	0.60	2.67	31.8
2Snβ-N_2/air	2.29	2.84	27.3
5Snβ-N_2/air	2.16	1.93	50.7
10Snβ-N_2/air	1.63	1.58	59.7

Table S3. Absorption depth (effect), difference (Δeffect) and reduced absorption depth difference (Δeffect/effect 77 K) values of the ^{119}Sn Mössbauer spectra of the different Snβ samples recorded at 77 K and RT.

Catalyst	effect 77 K (%)	effect RT (%)	Δeffect (%)	Δeffect/effect 77K (%)
2Snβ-air	8.5	3.9	4.6	54
5Snβ-air	9.5	4.0	5.5	58
10Snβ-air	8.5	4.6	3.9	46
2Snβ-N2/air	6.8	1.7	5.1	75
10Snβ-N2/air (3 h air)	7.6	2.0	5.6	74
10Snβ-N2/air (6 h air)	6.4	1.5	4.9	77

Table S4. The reported effective diffusivity in beta zeolites.

Compound	Zeolite	Crystal size (µm)	Effective Diffusivity (D_e) [m^2/s]	Temperature (°C)	Ref.
Benzene	H-beta	0.9	$3.2\ 10^{-13}$	80	[8]
Toluene	H-beta	0.9	$0.9\ 10^{-13}$	80	[8]
phenol	H-beta	1.1	$>1\ 10^{-14}$	n.m	[9]
Phenol	Al-free Ti-beta	2-5	$1.5\ 10^{-15}$	60	[10]
Benzyl alcohol	H-beta	10	10^{-13}	25	[11]

References

(1) Li, P.; Liu, G.; Wu, H.; Liu, Y.; Jiang, J.; Wu, P. Postsynthesis and Selective Oxidation Properties of Nanosized Sn-Beta Zeolite. *J. Phys. Chem. C* **2011**, *115* (9), 3663–3670. https://doi.org/10.1021/jp1076966.

(2) Harris, J. W.; Cordon, M. J.; Iorio, J. R. Di; Vega-Vila, J. C.; Ribeiro, F. H.; Gounder, R. Titration and Quantification of Open and Closed Lewis Acid Sites in Sn-Beta Zeolites That Catalyze Glucose Isomerization. *J. Catal.* **2016**, *335*, 141–154. https://doi.org/https://doi.org/10.1016/j.jcat.2015.12.024.

(3) Wallace, W. E. Mass Spectra. In *NIST Chemistry WebBook, NIST Standard Reference Database number 69*; National Institue of Standards and Technology, Gaithersburd MD, 20899. https://doi.org/10.18434/T4D303.

(4) Crépeau, G.; Montouillout, V.; Vimont, A.; Mariey, L.; Cseri, T.; Maugé, F. Nature, Structure and Strength of the Acidic Sites of Amorphous Silica Alumina: An IR and NMR Study. *J. Phys. Chem. B* **2006**, *110* (31), 15172–15185. https://doi.org/10.1021/jp062252d.

(5) Onfroy, T.; Clet, G.; Houalla, M. Quantitative IR Characterization of the Acidity of Various Oxide Catalysts. *Microporous Mesoporous Mater.* **2005**, *82* (1), 99–104. https://doi.org/https://doi.org/10.1016/j.micromeso.2005.02.020.

(6) Di Iorio, J. R.; Johnson, B. A.; Román-Leshkov, Y. Ordered Hydrogen-Bonded Alcohol Networks Confined in Lewis Acid Zeolites Accelerate Transfer Hydrogenation Turnover Rates. *J. Am. Chem. Soc.* **2020**, *142* (45), 19379–19392. https://doi.org/10.1021/jacs.0c09825.

(7) Joshi, H.; Ochoa-Hernández, C.; Nürenberg, E.; Kang, L.; Wang, F. R.; Weidenthaler, C.; Schmidt, W.; Schüth, F. Insights into the Mechanochemical Synthesis of Sn-β: Solid-State Metal Incorporation in Beta Zeolite. *Microporous Mesoporous Mater.* **2020**, 110566. https://doi.org/https://doi.org/10.1016/j.micromeso.2020.110566.

(8) Roque-Malherbe, R.; Wendelbo, R.; Mifsud, A.; Corma, A. Diffusion of Aromatic Hydrocarbons in H-ZSM-5, H-Beta, and H-MCM-22 Zeolites. *J. Phys. Chem.* **1995**, *99* (38), 14064–14071. https://doi.org/10.1021/j100038a043.

(9) Linh, T. N.; Fujita, H.; Sakoda, A. Diffusion of Non-Volatile Phenolic Compounds in Zeolite Beta and Silicalite in Liquid Phase. *Adsorption* **2016**, *22* (7), 1001–1011. https://doi.org/10.1007/s10450-016-9808-7.

(10) Wilkenhöner, U.; Gammon, D. W.; van Steen, E. Intrinsic Activity of Titanium Sites in TS-1 and

Al-Free Ti-Beta. In *Impact of Zeolites and other Porous Materials on the new Technologies at the Beginning of the New Millennium*; Aiello, R., Giordano, G., Testa, F., Eds.; Studies in Surface Science and Catalysis; Elsevier, 2002; Vol. 142, pp 619–626. https://doi.org/https://doi.org/10.1016/S0167-2991(02)80081-7.

(11) Chiu, J. J.; Pine, D. J.; Bishop, S. T.; Chmelka, B. F. Friedel–Crafts Alkylation Properties of Aluminosilica SBA-15 Meso/Macroporous Monoliths and Mesoporous Powders. *J. Catal.* **2004**, *221* (2), 400–412. https://doi.org/https://doi.org/10.1016/j.jcat.2003.09.005.